Emerging trends in heavy precipitation and hot temperature extremes in Switzerland

S. C. Scherrer[1], E. M. Fischer[2], R. Posselt[1], M. A. Liniger[1], M. Croci-Maspoli[1], and R. Knutti[2]

[1]Federal Office for Meteorology and Climatology MeteoSwiss, Zurich, Switzerland, [2]Institute for Atmospheric and Climate Science, ETH Zurich, Zurich, Switzerland

Abstract Changes in intensity and frequency of daily heavy precipitation and hot temperature extremes are analyzed in Swiss observations for the years 1901–2014/2015. A spatial pooling of temperature and precipitation stations is applied to analyze the emergence of trends. Over 90% of the series show increases in heavy precipitation intensity, expressed as annual maximum daily precipitation (mean change: +10.4% 100 years^{-1}; 31% significant, $p < 0.05$) and in heavy precipitation frequency, expressed as the number of events greater than the 99th percentile of daily precipitation (mean change: +26.5% 100 years^{-1}; 35% significant, $p < 0.05$). The intensity of heavy precipitation increases on average by 7.7% K^{-1} smoothed Swiss annual mean temperature, a value close to the Clausius-Clapeyron scaling. The hottest day and week of the year have warmed by 1.6 K to 2.3 K depending on the region, while the Swiss annual mean temperature increased by 1.9 K. The frequency of very hot days exceeding the 99th percentile of daily maximum temperature has more than tripled. Despite considerable local internal variability, increasing trends in heavy precipitation and hot temperature extremes are now found at most Swiss stations. The identified trends are unlikely to be random and are consistent with climate model projections, with theoretical understanding of a human-induced change in the energy budget and water cycle and with detection and attribution studies of extremes on larger scales.

1. Introduction

Climate change affects the mean climate, but also weather extremes, which often have large socioeconomic impacts and are of vital importance for an integrated climate risk management [*Adger*, 2009; *World Meteorological Organization* (*WMO)*, 2015]. The frequency and intensity of hot temperatures and heavy precipitation have increased on global and continental scales [*Alexander et al.*, 2006; *Donat et al.*, 2013; *Klein Tank and Können*, 2003; *Perkins et al.*, 2012; *Rahmstorf and Coumou*, 2011; *Fischer and Knutti*, 2014; *Zwiers et al.*, 2011] and are projected to increase in the future in most parts of the world [*Sillmann et al.*, 2013; *Kharin et al.*, 2013; *Orlowsky and Seneviratne*, 2011; *Fischer et al.*, 2014; *Fischer et al.*, 2013; *Seneviratne et al.*, 2016] and in Switzerland [*CH2011*, 2011; *Schär et al.*, 2004; *Frei et al.*, 2006; *Rajczak et al.*, 2013; *Fischer et al.*, 2015]. Large-scale and subcontinental trends in some extremes have been attributed to human influence [*Stott et al.,* 2004, 2010; *Min et al.*, 2013; *Morak et al.*, 2013; *Fischer and Knutti*, 2015; *Zhang et al.*, 2013; *Christidis et al.*, 2011, 2015]. Also, from a physical perspective there is evidence that hot temperature and heavy rainfall extremes will become more frequent and more extreme in a warmer world [*Boucher et al.*, 2013; *O'Gorman and Schneider*, 2009]. The water content of the atmosphere, for example, has been found to scale roughly at the Clausius-Clapeyron rate of 6–7% K^{-1} [e.g., *Trenberth et al.*, 2003]. Many studies investigated the scaling of heavy precipitation with temperature in observations for different time scales [e.g., *Westra et al.*, 2013; *Allan and Soden*, 2008; *Lenderink and van Meijgaard*, 2008]. Most of them found scalings relatively close to the Clausius-Clapeyron rate, except for subdaily such as hourly rainfall where some studies reported higher scaling rates [e.g., *Berg et al.*, 2013; *Lenderink and van Meijgaard*, 2008; *Westra et al.*, 2014]. At the local scale however, relatively small trends in precipitation extremes could still be hidden or amplified by large natural variability [*Frei and Schär*, 2001; *Fischer et al.*, 2013]. Recent studies found that globally about two thirds of the stations and grid points in gridded data sets experienced increases in the intensity of extreme precipitation on the annual time scales during the twentieth century [*Westra et al.*, 2013; *Min et al.*, 2011]. It has also been shown that there is a positive scaling with global mean temperature [*Westra et al.*, 2013; *Min et al.*, 2011; *O'Gorman*, 2015]. Hot temperature extremes are increasing in most parts of the world [*Alexander et al.*, 2006; *Donat et al.*, 2013; *Perkins et al.*, 2012], but it is not entirely clear whether at similar rates as mean temperature [*Della-Marta et al.*, 2007; *Yiou et al.*, 2009; *Donat and Alexander*, 2012].
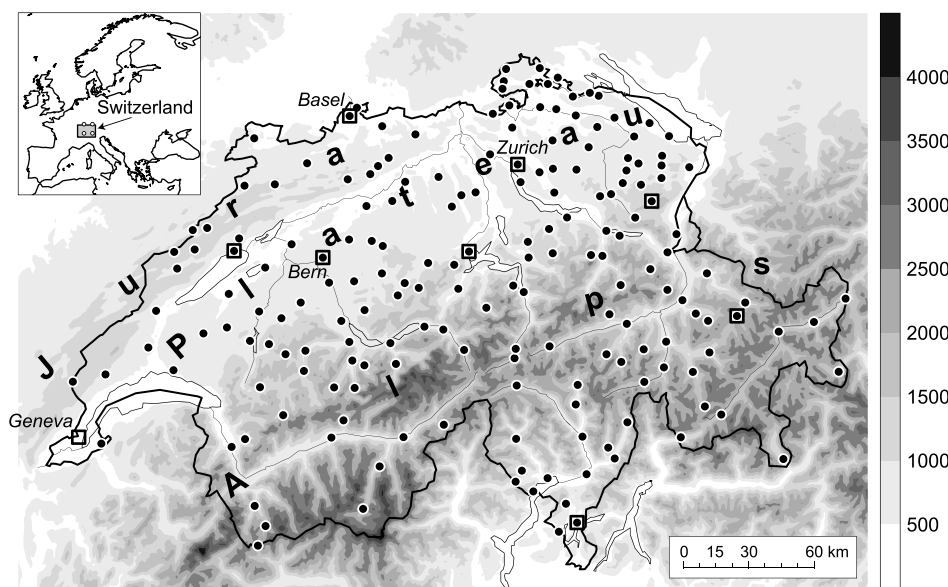
Figure 1. Map of Swiss precipitation stations (circles) and maximum temperature stations (squares) used. The grey shading shows the topography of Switzerland in meters above sea level. The three main regions, Jura mountains (~10% of Swiss area), Plateau (~30% of Swiss area), and Alps (~60% of Swiss area), are marked. The inset in the top left corner shows the location of Switzerland within Europe (grey square). The four dots in and close to the Swiss square show the four grid points of the global climate models used.

In this study we present strong evidence that trends in heavy precipitation, and hot temperature extremes are emerging from natural variability also on the spatial scale of the small country of Switzerland, i.e., are unlikely to be random. Several earlier studies found some indications for changes in daily Swiss temperature and precipitation extremes [*Courvoisier*, 1998; *Frei and Schär*, 2001; *Beniston and Stephenson*, 2004; *Schmidli and Frei*, 2005; *Salzmann et al.*, 2015]. However, the influence of interannual to decadal variability on trend evolution was not specifically addressed, and most of the studies on precipitation did not include data of the most recent 10–20 years. Also, the increasing availability of climate model simulations makes it now possible to compare the observed trends with modeling results for the same period. We here present maps and distributions of observed trends in heavy precipitation frequency and intensity in the 1901 to 2014 period as well as hot temperature extremes in the 1901 to 2015 period using climate indices; some of them proposed by the WMO Expert Team on Climate Change Detection and Indices (ETCCDI) [*Zhang et al.*, 2011]. We quantify how the trends in heavy precipitation and hot temperature extremes scale with global and local mean temperature. The observed trends and trend scalings are pooled together and finally put into context of global climate model simulations for the past and the future climate.

2. Data and Methods

In this paper we shed light on the evolution of heavy precipitation and hot temperature extremes in terms of intensities and frequencies. To analyze changes in heavy precipitation, we use quality-checked but not homogenized daily precipitation sums from 185 spatially well-distributed MeteoSwiss stations covering the period 1901 to 2014. Figure 1 shows a map of the precipitation station locations (circles). Considering only quality-checked daily precipitation data is probably better than using the homogenized daily series since the homogenization procedure applied was designed to correct monthly precipitation sums and not to produce correct daily values of heavy precipitation days. A long analysis period of over 100 years has been chosen to get more clear signals from climate change and to minimize the influence of interannual and decadal variability. The starting year 1901 was chosen since high-quality data for a large number of Swiss stations are available since then. The (i) annual maxima of daily precipitation (Rx1day) is used as an index of changes in heavy precipitation intensity and (ii) the annual number of precipitation days exceeding the 99th percentile of daily precipitation (#R99e, considering days with and without precipitation) as index for changes in heavy precipitation frequency. The 99th percentile limits (i.e., values of events that occur on
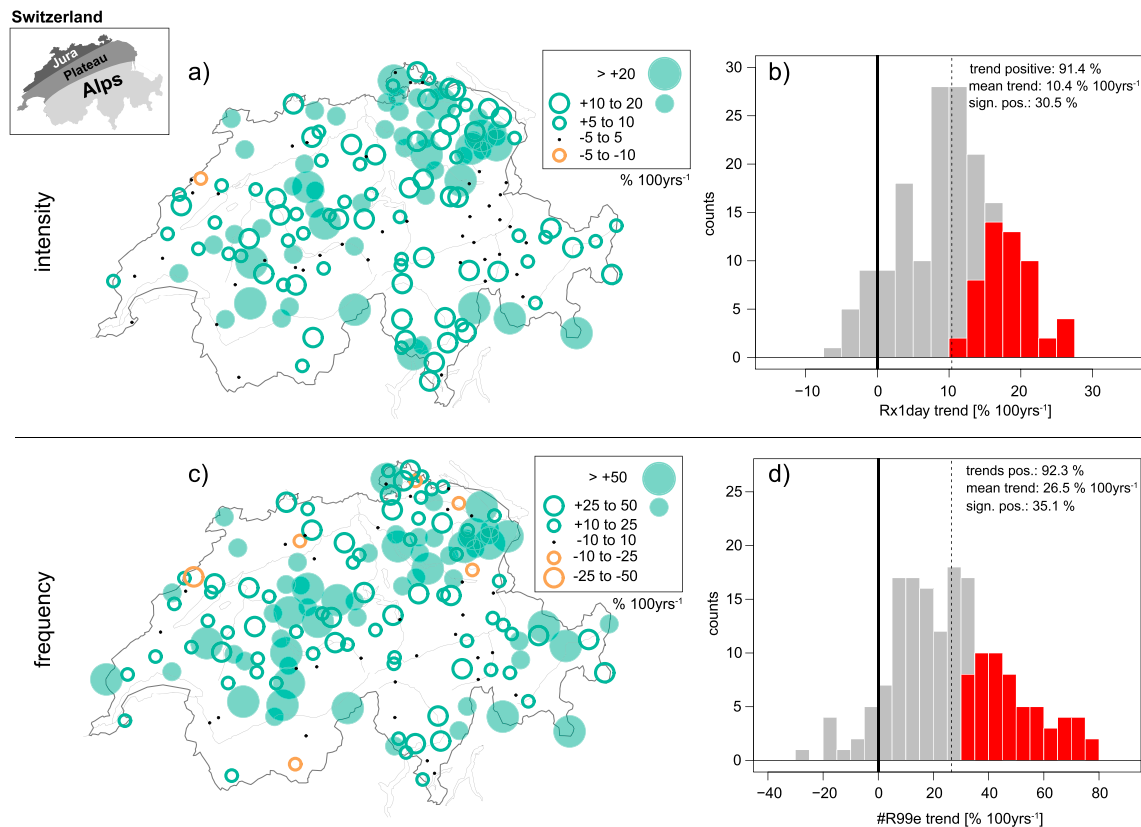
Figure 2. (a and b) Observed 1901–2014 trends of the annual daily maximum precipitation (Rx1day) and (c and d) the number of days exceeding the 99th percentile (#R99e) at ~170 Swiss precipitation stations, in % 100 yr s^{-1}. Filled circles and red histogram bars indicate trends that are statistically significant at the 5% level. The main geographical regions of Switzerland are shown in the inset on the top left corner.

average every 100 days) have been determined across all days in the 1961–1990 period. This choice avoids sampling uncertainties inherent to daily percentiles [*Mahlstein et al.*, 2015] and can be motivated by an only moderate seasonal cycle in Switzerland for daily precipitation. The 99th percentile threshold of daily precipitation varies between less than 25 mm d^{-1} in northern Switzerland and more than 100 mm d^{-1} at some stations in southern Switzerland. The number of actual days exceeding these values in a single year varies between 0 and roughly 10 days in the 1901–2014 series. Precipitation indices are only computed for series with less than 5 years of missing data in the 1901–2014 period, reducing the number of stations for trend analysis to about 170 on the annual and seasonal scale.

To investigate changes in hot temperature extremes, homogenized daily maximum temperature data [*Begert et al.*, 2005] from nine long and complete MeteoSwiss stations covering all major climate regions of Switzerland are used (cf. Figure 1, squares). The anomalies of all nine temperature series are used to create a "Swiss" series which is very highly correlated with the official Swiss mean temperatures series used by MeteoSwiss for national assessments. The official Swiss series is only available for mean temperature and cannot be used here. A four station mean (stations Zurich, Geneva, Basel, and Bern) is used as a proxy for the densely populated "Plateau" (cf. Figure 1 and Figure 2, inset). We restrict the analysis to the Swiss and Plateau series since the series are too similar in order to expect a meaningful spatial pattern.

The observational analysis period for hot temperature extremes is from 1901 to summer 2015. The following indices are used to investigate changes in hot temperature extreme intensities: the annual temperature maximum (i.e., the hottest day, abbreviated as TXx) and the annual maximum of averaged daily maximum temperature over a continuous N day period (abbreviated as TXx[N]d), where [N] is 3 and 7 (i.e., the hottest three day period and the hottest week). Additional indices are used to estimate changes in hot temperature extreme frequencies: the number days when daily maximum temperature is above the 90th, 95th, and 99th percentile (abbreviated as TX[P]p, where [P] is 90, 95, and 99). The TX[P]p indices have been computed using the R-package

climdex.pcic, which uses the resampling procedure suggested by *Zhang et al.* [2005] to avoid inhomogeneities in the temperature extremes. As reference period the 1961–1990 period was chosen, and only the summer months June, July, and August have been considered. Note that Rx1day, TXx, and TX90p are indices proposed by the ETCCDI [*Zhang et al.*, 2011]. A small difference is that we analyze the number of days instead of the percentage of days in the TX[*P*]p indices.

In this study, we scale the changes in heavy precipitation and hot temperature extremes to (i) global mean near-surface temperature (GMT) for ocean and land surface from the HadCRUT4 data set (version 4.3 [*Morice et al.*, 2012]) and (ii) the 30 year Gaussian smoothed Swiss annual mean temperature (sSAT) based on 12 long Swiss series [cf. *Begert et al.*, 2005]. This scaling with GMT allows to compare the results with other studies on the larger scale [e.g., *Seneviratne et al.*, 2016; *Westra et al.*, 2013], whereas the comparison with sSAT allows a somewhat more physical interpretation with the local changes.

For the continuous variables (e.g., Rx1day, TXx[*N*]d and their scalings) linear trends are computed using the robust method by Theil-Sen, and the trend significance is determined by the nonparametric Mann-Kendall trend test [*Yue and Pilon*, 2002]. For the count variables (e.g., #R99e, TX[*P*]p and their scalings), logistic trends are fitted to the data, and the changes are expressed as percentage changes (i.e., the fit for the year 2014 minus the fit for the year 1901 divided by the fit for the year 1901 multiplied by 100). Trends with *p* values less than 0.05 are classified as significant. To estimate the effects of interannual to decadal variability, we show moving-window analyses, i.e., the statistics of all possible consecutive 30 year windows between 1901 and 2014. Also note that we analyze the distribution of the trends but do not perform an emergence study in the strict sense as described in *Kirtman et al.* [2013].

In order to put the observed trends into a context with future projections, we also analyze temperature and precipitation extremes at four grid points of historical climate model simulations for the periods 1901–2005 as well as future projections forced with representative concentration pathway (RCP) 8.5 for the period 2006–2100. Note that due to differences in spatial scales, caution is needed when intensities of temperature extremes and particularly of precipitation extremes at a model grid box are compared with in situ station series. The absolute values of past precipitation extremes are generally substantially lower at a model grid box than at a station. However, the long-term relative trend of daily precipitation extremes per degree warming has been found to be reasonably consistent between model and observations and not strongly affected by the differences in spatial scales [*O'Gorman and Schneider*, 2009; *Westra et al.*, 2013]. Since the series here are still affected by internal variability, and the spatial correlation between neighboring stations is different than across neighboring model grid boxes, the trend histograms can only be compared in a qualitative way.

We explicitly use the models here to test whether the observed long-term trends are broadly consistent with model simulations rather than for a rigorous quantitative model evaluation. To assess the uncertainty present in current global climate models, we analyze one member from each of the 24 Coupled Model Intercomparison Project (CMIP5) models (cf. Table S1 in the supporting information) that provide the necessary daily output. The extreme indices are calculated on the native model grid and regridded using bilinear interpolation to a common grid. The regridding procedure has only a minor effect of the relative scaling of the intensity of precipitation extremes to global mean temperatures (cf. Figure S1). To get a first estimate of how much of the differences in trends can be explained by internal variability only, the simulations are supplemented with a 10 member ensemble performed with the Community Earth System Model (CESM) version 1.0.4 including the Community Atmosphere Model version 4 and fully coupled ocean, sea ice, and land surface components [*Hurrell et al.*, 2013; *Fischer et al.*, 2014]. The 10 members are initialized from different states of the preindustrial control simulation and differ in their initial conditions of the ocean, atmosphere, sea ice, and land components. Thereby the 10 CESM members share the exact same setup as the CMIP5 simulations. Note that the quantification of internal variability is model dependent, but the CESM estimates for Europe have been found to be consistent with reanalysis [*Fischer and Knutti*, 2013].

3. Observed Changes in Heavy Precipitation

3.1. Precipitation Intensity

The 1901–2014 trends in annual maximum precipitation intensity (Rx1day) are positive for 91% of the stations, with a mean trend of 10.4% 100 yr s^{-1} across all stations. The trends are largest and often significant
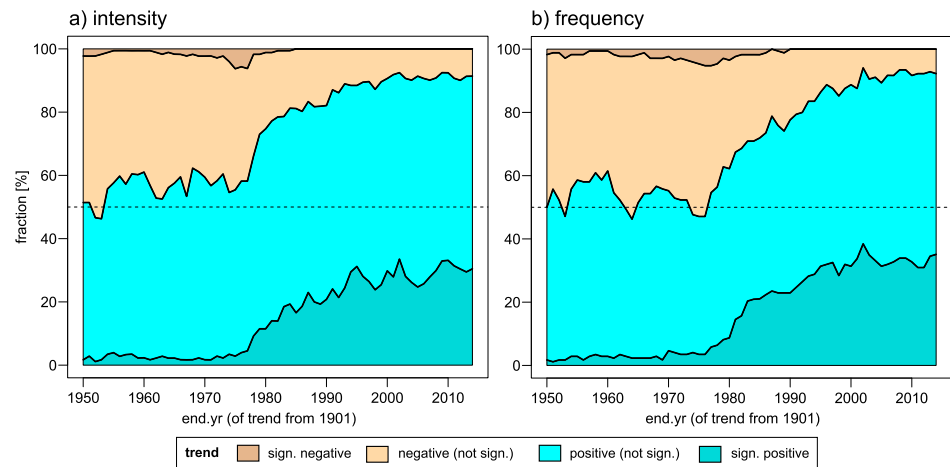
Figure 3. (a) Fraction (percentage) of trends (1901 to year on *x* axis) for daily heavy precipitation intensity (Rx1day) and (b) daily precipitation frequency (number of days exceeding the 99th percentile #R99e) at Swiss precipitation stations that show significant positive (dark blue), positive but nonsignificant (light blue), negative but nonsignificant (light brown), and significant negative (dark brown) trends (significance level: $p < 0.05$).

on the Swiss Plateau and the northern and southern slopes of the Alps (cf. Figure 2a). In the inner Alps, the trends are often relatively small and insignificant, but no clear altitude dependence is found (not shown). There is a considerable spread in the trends for the different stations, but 31% of the trends are significantly positive at the 5% level (Figure 2b). The annual and the summer map (Figures 2a and S2c) show similarities, since for most regions (e.g., Jura, Plateau, and northern slopes of the Alps), the annual precipitation maxima normally occur in summer. However, this does not mean that increasing trends in intensity in heavy precipitation are purely a summer feature. Increasing trends are found for all four seasons with 75% to 83% of the stations showing positive trends. The mean trends are +5.6% 100 yr s^{-1} in spring (March–May (MAM)), +8.1% 100 yr s^{-1} in winter (December–February (DJF)), +8.3% 100 yr s^{-1} in summer (June–August (JJA)) and +9.4% 100 yr s^{-1} in fall (September–November (SON)) (cf. Figures S3a and S2).

The fraction of 91% of Swiss stations showing positive Rx1day trends on the annual scale in the 1901–2014 period is much higher than the 64% found globally using 8326 worldwide stations in the 1900–2009 period [*Westra et al.*, 2013] or the 65% of grid boxes with positive trends in the HadEX gridded extremes data set over the period 1951–1999 [*Min et al.*, 2011]. For the period 1951–1999, 87% of the Swiss stations show positive Rx1day trends. This is an indication that the Swiss numbers are indeed higher, consistent with the stronger than average warming and not only due to the different record lengths or periods used in the different data sets. To put the Swiss number into context, we investigate the fraction of positive and negative Swiss trends as a function of trend length. Figure 3a shows the percentage of stations showing positive, significantly positive, negative, and significantly negative trends for the trends staring 1901 and ending in the years between 1950 and 2014. Until the mid-1970s, roughly half of the Swiss trends beginning in 1901 are positive, and half are negative, and the fraction of significant trends is very small. From the mid-1970s to 2000, the fraction of positive trends increases relatively quickly to about 90% and then remains stable until 2014. The mean level of Rx1day values is indeed clearly higher in the period from the late 1970s to 2014 than before with the year 1978 showing by far the largest Rx1day values on a large scale (caused by the 7–8 August 1978 event) [e.g., *Courvoisier et al.*, 1979]. We speculate that this nonlinear behavior is a combination of the overlaying effects of decadal variability and climate change. A detailed analysis however is beyond the scope of this study. Note that on the seasonal scale *Frei and Schär* [2001] and *Schmidli and Frei* [2005] also identified some spatially coherent and statistically significant trends for indices of heavy precipitation intensity and frequency. It has to be kept in mind that a smaller region is likely to exhibit more coherent structures in trends due to the spatial dependencies.

3.2. Heavy Precipitation Frequency

The 1901–2014 trends in annual heavy precipitation frequency (#R99e) are positive for 92% of the stations, with a mean trend of 26.5% 100 yr s^{-1} across all stations. The trends show a considerable spread from station
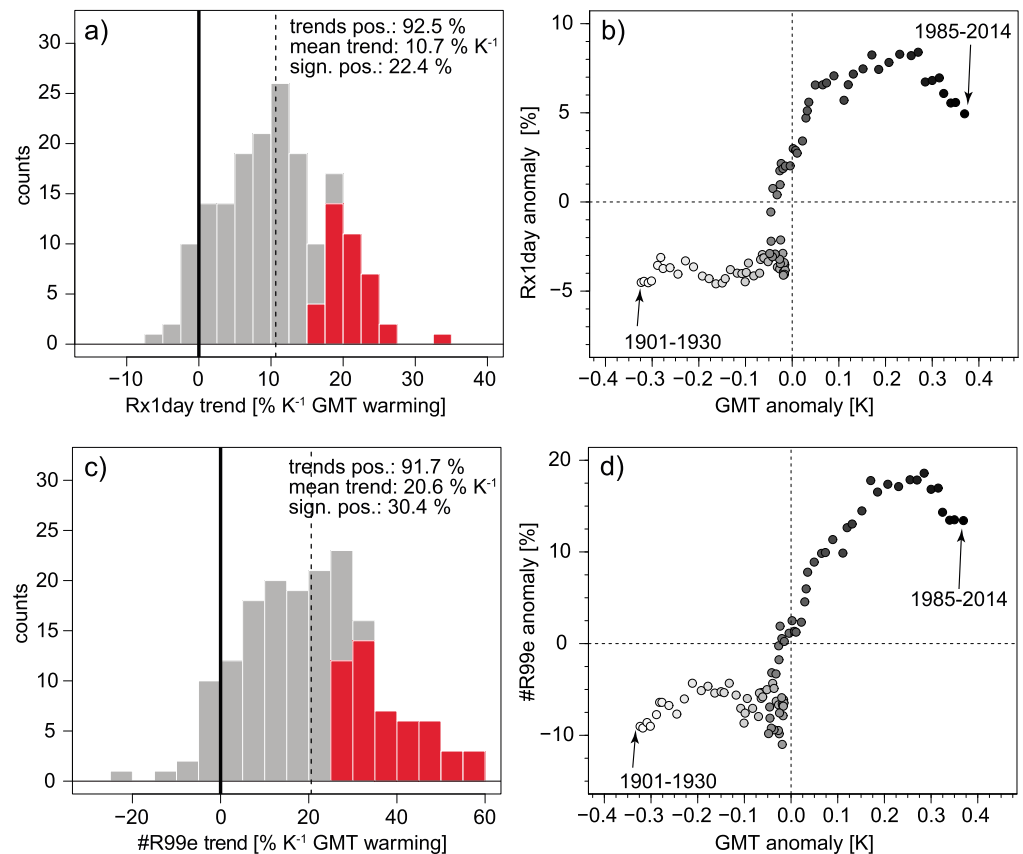
Figure 4. (a and b) Scaling of annual daily maximum precipitation Rx1day and (c and d) the number of days exceeding the 99th percentile #R99e with global mean temperature (GMT) for Swiss precipitation stations. Figures 4a and 4c: Histograms of percentage increase per Kelvin for the 1901–2014 period. The vertical dashed line shows the mean; red bars indicate values that are statistically significant at the 5% level. Figure 4b: GMT versus the all-station mean Rx1day anomaly (with respect to 1901–2014 mean) for all 30 year moving windows in the 1901–2014 period. Figure 4d: Same as Figure 4b but for #R99e.

to station, but 35% of the trends are significantly positive at the 5% level (cf. Figure 2d). No significantly negative trends are found. Trends tend to be largest toward the northern slopes of the Alps, a region prone to thunderstorms in summer (Figure 2c). The seasonal trends in summer (JJA) show a similar geographical pattern (Figure S4c) indicating that the increase in annual #R99e is probably dominated by more strong summer precipitation events. However, increasing trends are found for all four seasons with 72 to 87% of the stations showing positive trends. The mean trends are $+22.7\%$ $100\,\mathrm{yr\,s}^{-1}$ in winter (DJF), $+26.0\%$ $100\,\mathrm{yr\,s}^{-1}$ in summer (JJA), $+30.9\%$ $100\,\mathrm{yr\,s}^{-1}$ in spring (MAM), and $+37.4\%$ $100\,\mathrm{yr\,s}^{-1}$ in fall (SON) (cf. Figures S3b and S4). The percentage of stations with positive and significantly positive trends is very similar for other quantile limits (e.g., 90th, 95th, 99.5th, and 99.9th quantile) [cf. Figure S5]. Similar to the changes in heavy precipitation intensity, the fraction of positive and negative trends in heavy precipitation frequency is roughly 50% each until the mid-1970s. From the mid-1970s, the fraction of positive trends increases strongly to more than 90% until approximately 2000 to 2010 (cf. Figure 3b). As for Rx1day, the quick increase in the fraction of positive trends can be explained by the clearly higher annual #R99e since the late 1970s.

3.3. Relation With Local and Global Mean Temperature

Figure 4a shows histograms of the slopes of linear least squares regressions (called scaling below) of local extreme precipitation intensity (Rx1day) with annual global mean temperature (GMT) in the 1901–2014 period. The scaling with Rx1day is positive for 92% and significantly positive for 22% of the stations with a mean increase of $10.7\%\,\mathrm{K}^{-1}$ GMT. The mean scaling is a bit larger than the roughly $7\%\,\mathrm{K}^{-1}$ GMT found for global data sets [*Westra et al.*, 2013; *Min et al.*, 2011] and consistent with the local warming being stronger than on global average. The range of the ~170 Swiss scalings (roughly $-5\%\,\mathrm{K}^{-1}$ to $+35\%\,\mathrm{K}^{-1}$) is considerably

smaller than the one of *Westra et al.* [2013] for the global scale and over 8000 stations (values between roughly $-70\% \, K^{-1}$ and $>100\% \, K^{-1}$, cf. their Figure 10). Figure 4b shows the evolution in GMT anomaly versus the all-station mean Rx1day anomaly for 30 year moving windows (i.e., 1901–1930, 1902–1931,…, and 1985–2014). Rx1day anomalies are, in general, positively related with GMT, although the relation is superimposed by a lot of noise leading in parts to strong increases followed by no changes or even slight negative changes. There are similarities with the nonlinear behavior in the fraction of stations showing positive trends in Figure 3. We speculate that also here this is due to natural variability which is typically large for 30 year series of precipitation. Also, the scaling of seasonal heavy precipitation intensity with GMT is, in general, positive with a mean scaling between 7.1 and $17.0\% \, K^{-1}$ GMT depending on the season (Figure S6a). Finally, we find that the Rx1day anomalies also scale well with 30 year smoothed Swiss annual mean temperature (sSAT). The values are quite similar to the one with GMT with a tendency to somewhat lower numbers (mean scaling: $+7.7\% \, K^{-1}$ sSAT, which is very close to Clausius-Clapeyron scaling, and 16% of the stations showing significantly positive trends, Figure S7a).

The frequency of strong precipitation events (#R99e) also scales well with global mean temperature (cf. Figures 4c and 4d). The scaling is positive for 92% and significantly positive for 30% of the stations with a mean increase of $20.6\% \, K^{-1}$. The scaling of seasonal heavy precipitation frequency with GMT is, in general, positive with a mean scaling between 14.5 and $33.5\% \, K^{-1}$ GMT depending on the season (Figure S6b). As for heavy precipitation intensity, the scaling of the changes in frequency with 30 year smoothed Swiss annual mean temperature is very similar compared to scaling against GMT with a tendency to somewhat higher numbers (mean scaling: $+26.7\% \, K^{-1}$ sSAT and 35% of the stations showing significantly positive trends, Figure S7b).

4. Observed Changes in Hot Temperature Extremes

4.1. Hot Temperature Extreme Intensity

First, we present time series and trends of the three hot period intensity indices TXx, TXx3d, and TXx7d for the period 1901–2015. Figure 5a depicts the Swiss and Figure 5b the "Swiss Plateau" series. The top 5 years regarding the hottest days (TXx, red in Figure 5) are 2003, 2015, 1983, 1947, and 1921 for both, the Swiss and the Swiss Plateau. The 2015 and 2003 show the highest anomalies with very similar values. For the hottest week (TXx7d, blue in Figure 5) the top 5 years are 2003, 1947, 2015, 1952, and 1983. The 2003 shows clearly the highest anomalies, followed by 1947 ranking second and 2015 and ranking third. Using seasonal mean temperature, 2003 was by far the warmest summer, followed by 2015 (~1 K cooler than 2003) and 1994 which was again about 1 K cooler than 2015. The top ranked years coincide with all major Swiss summer heat waves and meteorological droughts documented in Switzerland since 1901 [*Calanca*, 2007; *Schär et al.*, 2004].

Interestingly, the hottest weeks of the Swiss series shows larger anomalies (~4 to almost 6 K) with respect to the 1901–2014 mean than the hottest day and 3 days periods in major heat wave years (i.e., 1947, 1952, 1983, 2003, and 2015). Also, the variance of the detrended TXx, TXx3d, and TXx7d series including all years is slightly increasing from daily to weekly time scales. An additional analysis of the hottest n day period time series 1901–2015 with $n = 1$ to 31 days shows that the variance is largest for n between about 5 and 12 days. For $n > 12$ days, the variance starts to decrease. We speculate that the larger variance of weekly anomalies might be related to synoptic variability and temperature feedback processes of rare but long-lasting blocking-like events causing such strong heat waves [e.g., *Barriopedro et al.*, 2011]. It would be worth to investigate this in detail, but this is beyond the scope of this study.

The 1901–2014 period trends of the hot temperature extreme "intensity" indices are all highly significant. On average, the increases in hot temperature extremes increase somewhat with the temporal length of the event (Swiss TXx:+1.9 K, TXx3d: +2.1 K, and TXx7d:+2.3 K) and are slightly larger for the Swiss series compared to the Swiss Plateau series (Figures 5a and 5b). Also shown in Figure 5a is the time series and trend (+1.9 K) of the mean temperature Tm. On the Swiss Plateau TXx and TXx7d increased from 31.5°C and 28°C in the early twentieth century to about 33°C and 30°C on average (Figure 5b).

4.2. Hot Temperature Extreme Frequencies

Beside changes in hot temperature extreme intensities (amplitudes of the hottest periods), also the change in the frequencies (how often very warm conditions occur during summer) is of interest. Figure 5c shows the
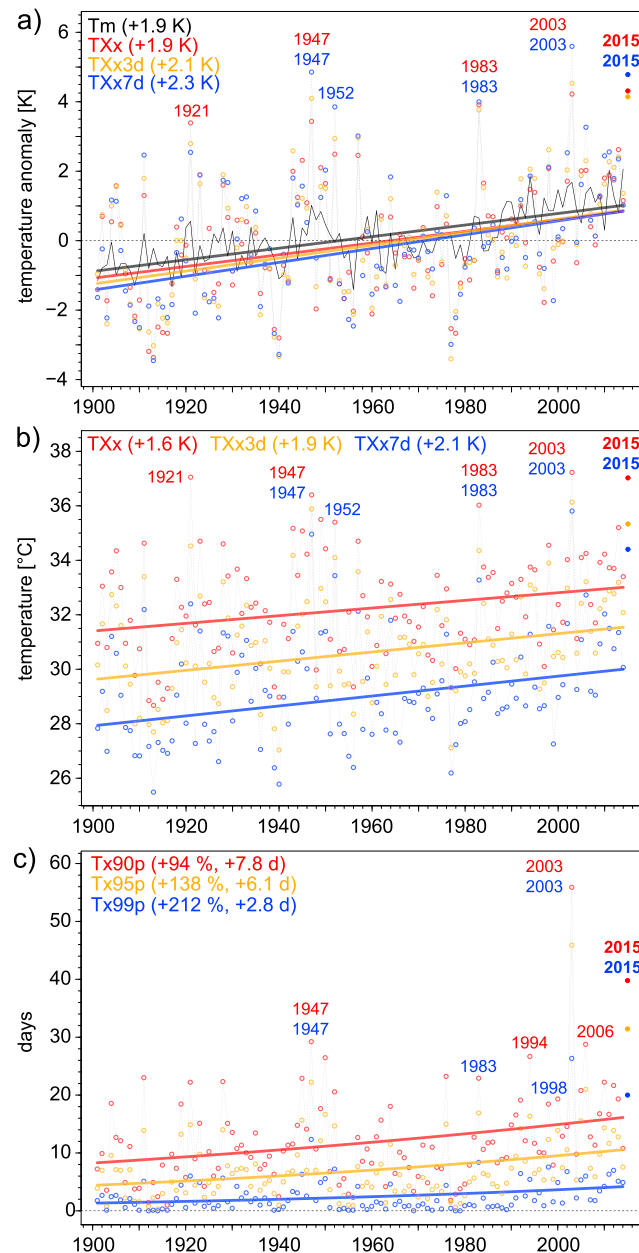
Figure 5. (a) The 1901–2014 anomalies and trends of TXx (red), TXx3d (orange), and TXx7d (blue) period of the year plus values of summer 2015 (filled dots) for the Swiss series. Black: annual mean temperature anomalies Tm. (b) Same as Figure 5a but showing absolute temperatures (in °C) for the densely populated Swiss Plateau. (c) Same as Figure 5a but showing the number of days and trends of TX90p (red), TX95p (orange), and TX99p (blue). The 1901–2014 trends are shown in the top left corner (Figures 5a and 5b: in K, Figure 5c: percentage and in days). The five record years of TXx and TX90p (red) as well as TXx7d and TX99p (blue) are labeled.

TX90p, TX95p, and TX99p time series for the Swiss series. The top 3 years regarding the TX90p days (red in Figure 5) are the same as for the intensities (2003, 2015, and 1947). The years ranking fourth and fifth (2006 and 1998) have not been in the top 5 years in terms of the hottest periods. For the rarer TX99p days, 2003, 2015, 1947, and 1983 rank first. Rank 5 is again a year that did not appear on the list of the hottest periods, namely, 1998. For all hot frequency indices, 2003 shows clearly the highest number of days above the percentile limits followed by summer 2015 and 1947.

The 1901–2014 period trends of the hot temperature extreme "frequency" indices are all highly significant ($p < 0.01$). The rarer the events, the stronger the increase (TX90p: +94% or +7.8 days, TX95p: +138% or +6.1 days, and TX99p: +212% or +2.8 days). The TX95p have more than doubled, and the TX99p days have more than tripled since 1901. These numbers are consistent with the findings based on heat wave indicator by *Della-Marta et al.* [2007] for western Europe and the period 1880–2005.

5. Comparison With Trends in Climate Models

The observed trends in heavy precipitation and temperature extremes raise the question whether these are consistent with the models that project a substantial future intensification of heavy precipitation and increasing hot temperatures along with rising global mean temperatures. Furthermore, it is interesting to understand whether the hypothesis that internal variability may alter existing underlying signals at certain locations is supported by climate models. While a direct quantitative model evaluation is hampered by the different spatial scales represented by model grid boxes and observational stations, we here use global climate models to put the observed trends in a broader context of large-scale anthropogenic climate change. We examine whether the observed trends fall within the range of past and future trends in global climate model simulations. Figure 6 shows the trends scaled with GMT for Rx1day and #R99e and the hottest day of the year (TXx) for the observations as well as the CMIP5 simulations. The CMIP5 distribution is composed of a sample of 96 (24 models times four grid points, see section 2 for details).
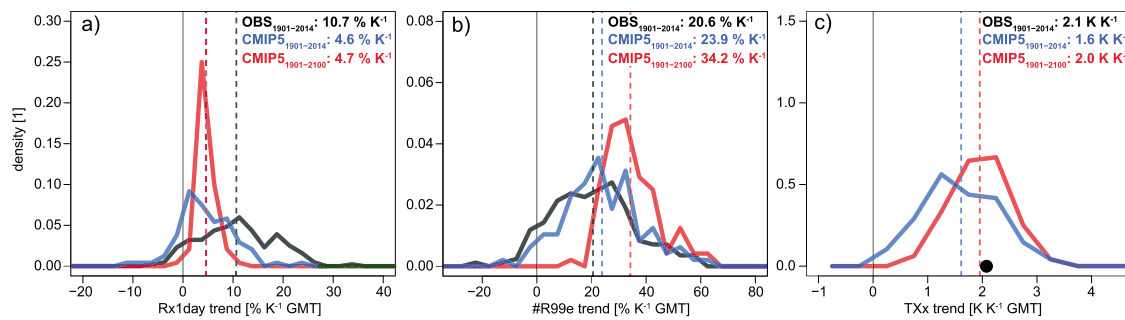
Figure 6. (a) Distributions of trends in Rx1day, (b) #R99e, and (c) TXx with GMT as predictor for the observations in the 1901–2014 period (solid black line for Rx1day and #R99e, black dot for TXx) and CMIP5 models for the 1901–2014 period (blue) and the 1901–2100 period (red). The mean values are shown as dashed lines, the numbers given in the upper right corner. The distributions show the station sample for observations ($n \sim 170$ for precipitation) and the model sample times grid points ($n = 96$) for the climate simulations. The black dot in Figure 6c is the mean of nine stations across Switzerland. Units: $\% \, K^{-1}$ GMT or $K \, K^{-1}$ GMT.

The observed trends in Rx1day over the historical period 1901–2014 are broadly consistent with the range of simulated trends. The simulated mean Rx1day trend across CMIP5 ($4.6\% \, K^{-1}$ GMT) is substantially smaller than those of the observations ($10.7\% \, K^{-1}$ GMT). This is consistent with the finding that the majority of CMIP5 models underestimate the observed intensification of heavy precipitation over Europe and the globe [*Min et al.*, 2011; *Zhang et al.*, 2013; *Fischer and Knutti*, 2014]. However, at the scale of Switzerland the differences between simulated and observed trends need to be interpreted with caution. The range of simulated and observed trends cannot be directly compared. The range of the observations is due to spatial variability, internal variability and sampling uncertainty. The simulated range reflects a combination of model uncertainty, internal variability, spatial variability across the four grid boxes and sampling uncertainty. Since the internal variability is strongly affected by the spatial scale, we do not expect that the observations and simulations show the same range. We find however that even at the relatively coarse grid boxes of the models internal variability plays an important role for trends longer than a century, since simulated trends across 10 realizations of one single model (CESM) [cf. Figure S8a] show an almost equally wide range of trends as the whole of CMIP5. Although the evaluation of trends at this scale is hampered by internal variability, we conclude that the observed intensification is at the high end of models that project a consistent long-term intensification of heavy precipitation over the period 1901–2100 (cf. Figure 6a; CMIP5 mean trend: $4.7\% \, K^{-1}$ GMT, see also *Kharin et al.* [2013]). Furthermore, the models confirm the hypothesis that underlying long-term signals may be masked by internal variability for trend length longer than a century.

In contrast to Rx1day, the mean simulated trend in #R99e of $23.9\% \, K^{-1}$ GMT is slightly higher than those of the observations ($20.6\% \, K^{-1}$ GMT, cf. Figure 6b). To some extent this may be due to the comparison of trends over large model grid boxes experiencing comparatively low variability against observed trends at stations experiencing high variability. While this scale differences is less critical for relative Rx1day changes, it complicates the comparison of trends in threshold exceedances such as #R99e. From the analysis it is difficult to disentangle the effect of variability and uncertainties coming from statistical trend estimates (especially for #R99e). *Frei and Schär* [2001] showed that trend estimation is nontrivial also for moderately rare events such as #R99e. The 10 realizations of the CESM ensemble for the 1901–2014 period show an even wider range than the CMIP5 ensemble (Figure S8b). For the 1901–2100 period, the trend ranges of the CESM and CMIP5 ensemble are similar (Figures 6b and S8b). The 1901–2100 CMIP5 trend mean is a bit higher (mean trend: $34.2\% \, K^{-1}$ GMT) than in the observational period.

The mean observed TXx trend ($+2.1 \, K \, K^{-1}$ GMT) lies well inside the CMIP5 trend range and relatively close to the CMIP5 mean estimates ($+1.6 \, K \, K^{-1}$ GMT) for the 1901–2014 period and $+2.0 \, K \, K^{-1}$ GMT) for 1901–2100, Figure 6c). The CESM ensemble TXx trend values are somewhat lower for the 1901–2014 period (mean: $+1.5 \, K \, K^{-1}$ GMT) and a bit higher for the 1901–2100 period (mean: $+2.6 \, K \, K^{-1}$ GMT), but the observed TXx trend is still inside the CESM trend range. Again, a detailed evaluation at the local scale is impossible due to the major role of internal variability [*Perkins and Fischer*, 2013], but the observed trends are consistent with models, which for a 2 K warmer world, project on average about 4 K warmer hot days over Switzerland.

6. Summary and Conclusions

Trends in the intensity and frequency of heavy precipitation and hot temperature extremes in Switzerland have been analyzed for the period 1901–2014/2015. We found that on the annual scale 91–92% of the Swiss precipitation stations show both trends to more frequent and more intense extreme precipitation with 31% and 35% of the trends, respectively, being statistically significant ($p < 0.05$). These numbers are much higher than the global numbers where about 65% of the stations or grid points show positive trends in precipitation intensity [cf. *Westra et al.*, 2013; *Min et al.*, 2011]. The highest annual 1 day precipitation sums (Rx1day) increased on average by 10.4% $100\,\mathrm{yr\,s}^{-1}$, while the number of days exceeding the 99th percentile of daily precipitation increased on average by +26.5% $100\,\mathrm{yr\,s}^{-1}$. The intensity of heavy precipitation expressed as Rx1day increases on average by +7.7% K^{-1} smoothed Swiss annual mean temperature, which is close to the Clausius-Clapeyron scaling.

The hottest 1, 3, and 7 day periods of the year have warmed by +1.9 to 2.3 K since 1901 for a Swiss average and by +1.6 to 2.1 K on the Swiss Plateau, similar to trends of annual mean temperature, which increased by +1.9 K over the same period. The number of moderate summer temperature extremes (TX90p) has roughly doubled (+94%); the more extreme TX99p days have more than tripled (+212%) since 1901. Trends over subperiods of 30 years show strong variations due to internal variability. However, the overall observed trends in heavy precipitation intensity and frequency as well as hot temperature extremes are well in line with those simulated by global climate models. The heat wave of summer 2015 will further contribute to this trend, with TXx values very similar to the record of summer 2003 but also with the second hottest week (TXx7d) and seasonal mean, exceeded only by the summer of 2003.

Trends in some weather extremes have been attributed to human-induced climate change on continental to global scales based on spatial pattern-based techniques [*Min et al.*, 2013; *Morak et al.*, 2013; *Fischer and Knutti*, 2015; *Zhang et al.*, 2013; *Christidis et al.*, 2011], but local trends are often dominated by internal variability. However, spatial pooling of stations can help to robustly identify emerging trends even in small countries. For Switzerland, increasing trends in hot days and heavy precipitation are now found at most stations. As expected from large natural variability on local scales, not all trends are significant but are expected to become significant as warming continues [*King et al.*, 2015]. This is consistent with earlier model projections and with the theoretical understanding of a human-induced signal in the energy budget and water cycle emerging from background variability. While we have not performed a formal attribution study, the trends over Switzerland as a whole are unlikely to be random and are fully consistent with anthropogenic climate change as simulated by climate models.

References

Adger, N. W. (2009), Social capital, collective action and adaptation to climate change, *Econ. Geogr.*, *79*, 387–404, doi:10.1111/j.1944-8287.2003.tb00220.x.

Alexander, L., et al. (2006), Global observed changes in daily climate extremes of temperature and precipitation, *J. Geophys. Res.*, *111*, D05109, doi:10.1029/2005JD006290.

Allan, R., and B. Soden (2008), Atmospheric warming and the amplification of precipitation extremes, *Science*, *321*, 1481–1484.

Barriopedro, D., E. M. Fischer, J. Luterbacher, R. M. Trigo, and R. García-Herrera (2011), The hot summer of 2010: Redrawing the temperature record map of Europe, *Science*, *332*, 220–224, doi:10.1126/science.1201224.

Begert, M., T. Schlegel, and W. Kirchhofer (2005), Homogeneous temperature and precipitation series of Switzerland from 1864 to 2000, *Int. J. Climatol.*, *25*, 65–80.

Beniston, M., and D. B. Stephenson (2004), Extreme climatic events and their evolution under changing climatic conditions, *Global Planet. Change*, *44*, 1–9, doi:10.1016/j.gloplacha.2004.06.001.

Berg, P., C. Moseley, and J. O. Haerter (2013), Strong increase in convective precipitation in response to higher temperatures, *Nat. Geosci.*, *6*, 181–185.

Boucher, O. D., et al. (2013), Clouds and Aerosols, in *Climate Change 2013: The Physical Science Basis. Contribution of Working Group I to the Fifth Assessment Report of the Intergovernmental Panel on Climate Change*, edited by T. F. Stocker et al., pp. 571–657, Cambridge Univ. Press, Cambridge, U. K., and New York.

Calanca, P. (2007), Climate change and drought occurrence in the Alpine region. How severe are becoming the extremes? *Global Planet. Change*, *57*, 151–160, doi:10.1016/j.gloplacha.2006.11.001.

CH2011 (2011), *Swiss Climate Change Scenarios CH2011*, pp. 88, C2SM, MeteoSwiss, ETH, NCCR Climate, and OcCC, Zurich, Switzerland.

Christidis, N., P. Stott, and S. Brown (2011), The role of human activity in the recent warming of extremely warm daytime temperatures, *J. Clim.*, *24*, 1922–1930.

Christidis, N., G. S. Jones, and P. A. Stott (2015), Dramatically increasing chance of extremely hot summers since the 2003 European heatwave, *Nat. Clim. Change*, *5*, 46–50, doi:10.1038/nclimate2468.

Courvoisier, H. W. (1998), Statistik der 24-stündigen Starkniederschläge in der Schweiz 1901–1996. SMA Report, 194, 20 pp. [Available at http://www.meteoschweiz.admin.ch.]

Courvoisier, H. W., G. Gensler, B. Primault, and H.-P. Rösli (1979), Das Unwetter vom 7. /8. August 1978 in der Schweiz. MZA Report, 85, 62 pp. [Available http://www.meteoschweiz.admin.ch.]

Della-Marta, P. M., M. R. Haylock, J. Luterbacher, and H. Wanner (2007), Doubled length of western European summer heat waves since 1880, *J. Geophys. Res.*, 112, D15103, doi:10.1029/2007JD008510.

Donat, M. G., and L. V. Alexander (2012), The shifting probability distribution of global daytime and night-time temperatures, *Geophys. Res. Lett.*, 39, L14707, doi:10.1029/2012GL052459.

Donat, M. G., et al. (2013), Updated analyses of temperature and precipitation extreme indices since the beginning of the twentieth century: The HadEX2 dataset, *J. Geophys. Res. Atmos.*, 118, 2098–2118, doi:10.1002/jgrd.50150.

Fischer, A. M., D. E. Keller, M. A. Liniger, J. Rajczak, C. Schär, and C. Appenzeller (2015), Projected changes in precipitation intensity and frequency in Switzerland: A multi-model perspective, *Int. J. Climatol.*, 35, 3204–3219, doi:10.1002/joc.4162.

Fischer, E. M., and R. Knutti (2013), Robust projections of combined humidity and temperature extremes, *Nat. Clim. Change*, 3, 126–130, doi:10.1038/nclimate1682.

Fischer, E. M., and R. Knutti (2014), Detection of spatially aggregated changes in temperature and precipitation extremes, *Geophys. Res. Lett.*, 41, 547–554, doi:10.1002/2013GL058499.

Fischer, E. M., and R. Knutti (2015), Anthropogenic contribution to global occurrence of heavy-precipitation and high-temperature extremes, *Nat. Clim. Change*, 5, 560–564, doi:10.1038/nclimate2617.

Fischer, E. M., U. Beyerle, and R. Knutti (2013), Robust spatially aggregated projections of climate extremes, *Nat. Clim. Change*, 3, 1033–1038, doi:10.1038/nclimate2051.

Fischer, E. M., J. Sedláček, E. Hawkins, and R. Knutti (2014), Models agree on forced response pattern of precipitation and temperature extremes, *Geophys. Res. Lett.*, 41, 8554–8562, doi:10.1002/2014GL062018.

Frei, C., and C. Schär (2001), Detection probability of trends in rare events: Theory and application to heavy precipitation in the Alpine region, *J. Clim.*, 14, 1568–1584.

Frei, C., R. Scholl, S. Fukutome, J. Schmidli, and P. L. Vidale (2006), Future change of precipitation extremes in Europe: Intercomparison of scenarios from regional climate models, *J. Geophys. Res.*, 111, D06105, doi:10.1029/2005JD005965.

Hurrell, J. W., et al. (2013), The Community Earth System model a framework for collaborative research, *BAMS*, 94, 1339–1360.

Kharin, V., F. Zwiers, X. Zhang, and M. Wehner (2013), Changes in temperature and precipitation extremes in the CMIP5 ensemble, *Clim. Change*, 119, 345–357.

King, A. D., M. G. Donat, E. M. Fischer, E. Hawkins, L. V. Alexander, D. J. Karoly, A. J. Dittus, S. C. Lewis, and S. E. Perkins (2015), The timing of anthropogenic emergence in climate extremes, *Environ. Res. Lett.*, 10, doi:10.1088/1748-9326/10/9/094015.

Kirtman, B., et al. (2013), Near-term climate change: Projections and predictability, in *Climate Change 2013: The Physical Science Basis. Contribution of Working Group I to the Fifth Assessment Report of the Intergovernmental Panel on Climate Change*, edited by T. F. Stocker et al., pp. 953–1028, Cambridge Univ. Press, Cambridge, U. K., and New York.

Klein Tank, A. M. G., and G. P. Können (2003), Trends in indices of daily temperature and precipitation extremes in Europe 1946–99, *J. Clim.*, 16, 3665–3680.

Lenderink, G., and E. van Meijgaard (2008), Increase in hourly precipitation extremes beyond expectations from temperature changes, *Nat. Geosci.*, 1, 511–514.

Mahlstein, I., C. Spirig, M. A. Liniger, and C. Appenzeller (2015), Estimating daily climatologies for climate indices derived from climate model data and observations, *J. Geophys. Res. Atmos.*, 120, 2808–2818, doi:10.1002/2014JD022327.

Min, S. K., X. Zhang, F. Zwiers, and G. C. Hegerl (2011), Human contribution to more-intense precipitation extremes, *Nature*, 470, 378–381.

Min, S., X. Zhang, F. Zwiers, H. Shiogama, Y. Tung, and M. Wehner (2013), Multimodel detection and attribution of extreme temperature changes, *J. Clim.*, 26, 7430–7451, doi:10.1175/JCLI-D-12-00551.1.

Morak, S., G. Hegerl, and N. Christidis (2013), Detectable changes in the frequency of temperature extremes, *J. Clim.*, 26, 1561–1574.

Morice, C. P., J. J. Kennedy, N. A. Rayner, and P. D. Jones (2012), Quantifying uncertainties in global and regional temperature change using an ensemble of observational estimates: The HadCRUT4 dataset, *J. Geophys. Res.*, 117, D08101, doi:10.1029/2011JD017187.

O'Gorman, P. A. (2015), Precipitation extremes under climate change, *Curr. Clim. Change Rep.*, 1, 49–59, doi:10.1007/s40641-015-0009-3.

O'Gorman, P. A., and T. Schneider (2009), The physical basis for increases in precipitation extremes in simulations of 21st-century climate change, *Proc. Natl. Acad. Sci. U.S.A.*, 106, 14,773–14,777, doi:10.1073/pnas.0907610106.

Orlowsky, B., and S. I. Seneviratne (2011), Global changes in extreme events: Regional and seasonal dimension, *Clim. Change*, doi:10.1007/s10584-011-0122-9.

Perkins, S. E., L. V. Alexander, and J. R. Nairn (2012), Increasing frequency, intensity and duration of observed global heatwaves and warm spells, *Geophys. Res. Lett.*, 39, L20714, doi:10.1029/2012GL053361.

Perkins, S. E., and E. M. Fischer (2013), The usefulness of different realizations for the model evaluation of regional trends in heatwaves, *Geophys. Res. Lett.*, 40, 5793–5797, doi:10.1002/2013GL057833.

Rahmstorf, S., and D. Coumou (2011), Increase of extreme events in a warming world, *Proc. Natl. Acad. Sci. U.S.A.*, 108, 17,905–17,909.

Rajczak, J., P. Pall, and C. Schär (2013), Projections of extreme precipitation events in regional climate simulations for Europe and the Alpine region, *J. Geophys. Res. Atmos.*, 118, 3610–3626, doi:10.1002/jgrd.50297.

Salzmann, N., S. C. Scherrer, S. Allen, and M. Rohrer (2015), Temperature, precipitation and related extremes in mountain areas, in *The High-Mountain Cryosphere—Environmental Changes and Human Risks*, edited by C. Huggel et al., pp. 28–49, Cambridge Univ. Press, Cambridge, U. K.

Schär, C., P. L. Vidale, D. Lüthi, C. Frei, C. Häberli, M. A. Liniger, and C. Appenzeller (2004), The role of increasing temperature variability in European summer heatwaves, *Nature*, 427, 332–336.

Schmidli, J., and C. Frei (2005), Trends of heavy precipitation and wet and dry spells in Switzerland during the 20th century, *Int. J. Climatol.*, 25, 753–771.

Seneviratne, S. I., M. G. Donat, A. J. Pitman, R. Knutti, and R. L. Wilby (2016), Allowable CO_2 emissions based on regional and impact-related climate targets, *Nature*, doi: 10.1038/nature16542.

Sillmann, J., V. Kharin, F. Zwiers, X. Zhang, and D. Bronaugh (2013), Climate extremes indices in the CMIP5 multimodel ensemble: Part 2. Future climate projections, *J. Geophys. Res. Atmos.*, 118, 2473–2493, doi:10.1002/jgrd.50188.

Stott, P. A., D. A. Stone, and M. R. Allen (2004), Human contribution to the European heatwave of 2003, *Nature*, 432, 610–614, doi:10.1038/nature03089.

Stott, P. A., N. P. Gillett, G. C. Hegerl, D. J. Karoly, D. A. Stone, X. Zhang, and F. Zwiers (2010), Detection and attribution of climate change: A regional perspective, *WIREs Clim. Change*, 1, 192–211, doi:10.1002/wcc.34.

Trenberth, K. E., A. Dai, R. M. Rasmussen, and D. B. Parsons (2003), The changing character of precipitation, *Bull. Am. Meteorol. Soc.*, 84, 1205–1217.

Westra, S., L. V. Alexander, and F. W. Zwiers (2013), Global increasing trends in annual maximum daily precipitation, *J. Clim.*, *26*, 3904–3918, doi:10.1175/JCLI-D-12-00502.1.

Westra, S., H. J. Fowler, J. P. Evans, L. V. Alexander, P. Berg, F. Johnson, E. J. Kendon, G. Lenderink, and N. M. Roberts (2014), Future changes to the intensity and frequency of short-duration extreme rainfall, *Rev. Geophys.*, *52*, 522–555, doi:10.1002/2014RG000464.

World Meteorological Organization (2015), Climate risk management. Accessed 17 August 2015. [Available at http://www.wmo.int/pages/themes/climate/risk_management_overview.php.]

Yiou, P., D. Dacunha-Castelle, S. Parey, and T. T. Huong Hoang (2009), Statistical representation of temperature mean and variability in Europe, *Geophys. Res. Lett.*, *36*, L04710, doi:10.1029/2008GL036836.

Yue, S., and G. Pilon (2002), Power of the Mann-Kendall and Spearman's rho tests for detecting monotonic trends in hydrological series, *J. Hydrol.*, *259*, 254–271.

Zhang, X., G. Hegerl, F. W. Zwiers, and J. Kenyon (2005), Avoiding inhomogeneity in percentile-based indices of temperature extremes, *J. Clim.*, *18*, 1641–1651, doi:10.1175/JCLI3366.1.

Zhang, X., L. Alexander, G. C. Hegerl, P. Jones, A. K. Tank, T. C. Peterson, B. Trewin, and F. W. Zwiers (2011), Indices for monitoring changes in extremes based on daily temperature and precipitation data, *WIREs Clim. Change*, *2*, 851–870, doi:10.1002/wcc.147.

Zhang, X., H. Wan, F. W. Zwiers, G. C. Hegerl, and S. K. Min (2013), Attributing intensification of precipitation extremes to human influence, *Geophys. Res. Lett.*, *40*, 5252–5257, doi:10.1002/grl.51010.

Zwiers, F. W., X. Zhang, and Y. Feng (2011), Anthropogenic influence on long return period daily temperature extremes at regional scales, *J. Clim.*, *24*, 881–892, doi:10.1175/2010JCLI3908.1.